Electronic Supplementary Material (ESI) for Communications.

Electronic Supplementary Information

Strong interfacial electronic coupling activates NiFeOOH for alkaline seawater oxidation

Bari Wulan,‡*[a], Weipeng Zhang,‡[a] Nana Chen,[a] Yuying Zhao,[a] Haibin Guan,[a] Jing Zhang,*[b] Dongxing Tan,[c] Lei Chen,*[a] Baofeng Zhao*[a]

[a] *Energy Research Institute, Shandong Key Laboratory of Clean and Efficient Biomass Energy Conversion and Utilization, Qilu University of Technology (Shandong Academy of Sciences), Jinan 250014 China. E-mail: bariwulan@qlu.edu.cn, zhaobf@sderi.cn*

[b] *Advanced Materials Institute, Qilu University of Technology (Shandong Academy of Sciences), Jinan 250014 China. E-mail: jingzhang@qlu.edu.cn*

[c] *Shandong Key Laboratory of Catalytic Conversion and Clean Energy, School of Chemistry and Chemical Engineering, Qufu Normal University, Qufu 273165 China.*

‡ These authors contributed equally to this work.

Experimental section

Materials and Chemicals

Nickel mesh (NM, 60 mesh), iron (III) nitrate nonahydrate ($Fe(NO_3)_3·9H_2O$), nickel (II) nitrate hexahydrate ($Ni(NO_3)_2·6H_2O$), gallium nitrate hydrate ($Ga(NO_3)_3·xH_2O$), potassium hydroxide (KOH), sodium chloride (NaCl), sodium hypophosphite monchydrate ($NaH_2PO_2·H_2O$), Ruthenium (IV) oxide (RuO_2), absolute methanol, hydrochloric acid (HCl) are purchased from Sinopharm Chemical Reagent Co., Ltd. FAA-3-PK-130 anion exchange membrane and commercial Pt/C catalysts were purchased from Suzhou Sinero tecnnologh Co., Ltd. The ultrapure water (18.2 MΩ·cm) was used in all experiments.

Preparation of Ni_2P/Fe_2P-Ga

In a typical synthesis, nickel mesh (NM) was ultrasonically cleaned in absolute ethanol, 3 M HCl, and deionized water for 10 min each, followed by drying under an Ar atmosphere. An aqueous precursor solution (100 mL) containing 0.4 mmol $Ni(NO_3)_2·6H_2O$, 0.1 mmol $Fe(NO_3)_3·9H_2O$, and x mmol $Ga(NO_3)_3·xH_2O$ (x = 0, 0.01, 0.1, and 0.2) was spray-deposited onto the NM placed on a hot plate maintained at 300°C. During deposition, compressed air at 0.2 MPa was used as the carrier gas, with the nozzle positioned 16 cm above the substrate, and the precursor solution was intermittently sprayed in cycles of 2 s on / 8 s off for 80 cycles to obtain NiFe-LDH-Ga. The coated substrates were subsequently phosphidized in a tube furnace under an Ar flow of 15 mL min^{-1}, with 0.4 g $NaH_2PO_2·H_2O$ placed upstream as the phosphorus source. The furnace was heated to 350°C at a ramping rate of 4°C min^{-1}, maintained for 2 h, and naturally cooled to room temperature to obtain Ni_2P/Fe_2P-Ga.

Preparation of NiFeOOH-GaO_x

Electrochemical activation was conducted by chronopotentiometry at 100 mA cm^{-2} for 1 h in a three-electrode configuration, with Ni_2P/Fe_2P-Ga, a graphite rod, and an Hg/HgO electrode serving as the working, counter, and reference electrodes, respectively. The activated Ni_2P/Fe_2P-Ga underwent in situ electrochemical oxidative reconstruction into the NiFeOOH-GaO_x phase. The average loading mass of the reconstructed NiFeOOH-GaO_x catalyst was estimated to be ~ 0.63 mg cm^{-2} from the mass difference of the nickel mesh before and after preparation.

Materials characterizations

The morphology and microstructures were systematically investigated by scanning electron microscopy (SEM, ZEISS GeminiSEM 300) and transmission electron microscopy (TEM, JEOL JEM-2100F). The phase composition was identified by X-ray diffraction (XRD, Bruker D8), and the surface chemical states and electronic structure were analyzed by X-ray photoelectron spectroscopy (XPS, Thermo Scientific ESCALAB 250Xi). Raman spectra were collected on a LabRAM Raman spectrometer with 532 nm laser excitation.

Electrochemical measurements

Electrochemical measurements were performed in a three-electrode configuration using a Donghua 7002A electrochemical workstation. A graphite rod and an Hg/HgO electrode served as the counter and reference electrodes, respectively. All potentials were converted to the reversible hydrogen electrode (RHE) scale. Linear sweep voltammetry (LSV) was recorded at a scan rate of 5 mV s^{-1}. Tafel slopes were obtained by fitting the Tafel equation ($\eta = a + b\log j$), where b is the slope and j is the current density. Electrochemical impedance spectroscopy (EIS) was conducted over a frequency range from 0.1 Hz to 100 kHz with an AC amplitude of 5 mV. The electrochemically active surface area (ECSA) was estimated from the double-layer capacitance (C_{dl}), which was derived from cyclic voltammetry (CV) collected at scan rates of 20, 40, 60, 80, and 100 mV s^{-1}. Simulated seawater electrolysis was further evaluated in an anion-exchange membrane (AEM) electrolyzer using Pt/C as the cathode (1 cm^2), NiFeOOH-Ga_2O_3 as the anode (1 cm^2), and an AEM separator (Fumasep FAA-3-PK-130).

Computational details

All density functional theory (DFT) calculations were performed using the projector-augmented wave (PAW) method as implemented in the Vienna Ab initio Simulation Package (VASP). The exchange-correlation interaction was described by the generalized gradient approximation (GGA) with the Perdew-Burke-Ernzerhof (PBE) functional, and long-range dispersion was included using the DFT-D3 correction. A plane-wave kinetic-energy cutoff of 400 eV was employed, and the electronic self-consistent field iterations were converged to 1×10^{-5} eV. A 15 Å vacuum layer was added to avoid the interaction between periodic cells. All structures were relaxed until

the residual force on each atom was below 0.03 eV/Å.

Under alkaline OER conditions, NiFe-LDH undergoes (de)protonation and oxidation to form Ni(Fe)OOH active phases. An LDH-derived layered NiFe (oxy)hydroxide slab was used as the structural model for the active surface. Considering the amorphous/non-stoichiometric nature of GaO_x and the absence of a unique atomic configuration, a Ga_2O_3 cluster was adopted as a simplified yet representative local structural motif of GaO_x to preserve the essential Ga^{3+}-O coordination environment and evaluate its interfacial interaction with the NiFeOOH surface. Accordingly, the Ga_2O_3 cluster was constructed on the exposed surface of the NiFe (oxy)hydroxide slab to obtain the NiFeOOH-GaO_x model. The Gibbs free-energy change (ΔG) of each elementary step was evaluated using the computational hydrogen electrode (CHE) model:

$$\Delta G = \Delta E + \Delta ZPE - T\Delta S$$

where ΔE is obtained directly from DFT calculations, ΔZPE is the change in zero-point energy, T is 298.15 K, and ΔS is the entropy change between products and reactants. Standard ideal gas methods were employed to calculate ZPE and TS energy correction. For adsorbates, all 3N degrees of freedom were treated as frustrated harmonic vibration with the catalyst surface set to be fixed during the calculation.

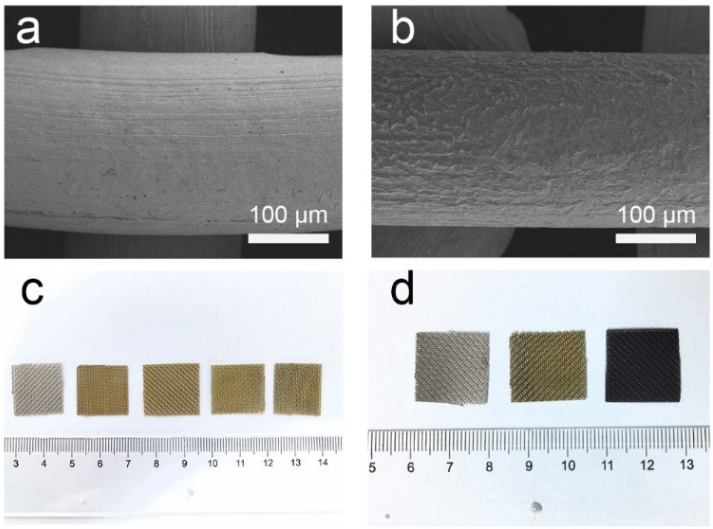

Fig. S1 SEM images of (a) pristine Ni mesh and (b) NiFe LDH-Ga deposited on Ni mesh by pulsed spray pyrolysis deposition (PSPD). Photographs of (c) NiFe LDH with different Ga contents and (d) the corresponding products after phosphidation.

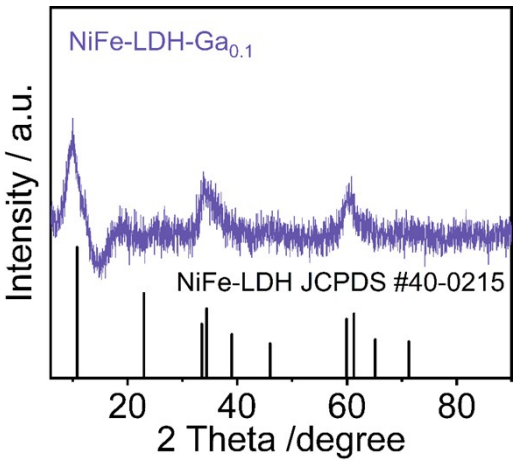

Fig. S2 XRD pattern of NiFe-LDH-$Ga_{0.1}$ deposited on a blank quartz substrate.

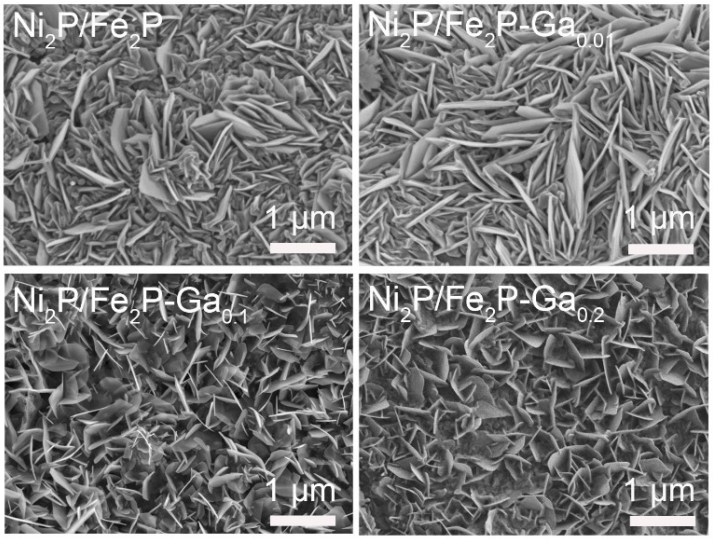

Fig. S3 SEM images of Ni_2P/Fe_2P-Ga_x: (a) x = 0, (b) x = 0.01, (c) x = 0.1, (d) x = 0.2.

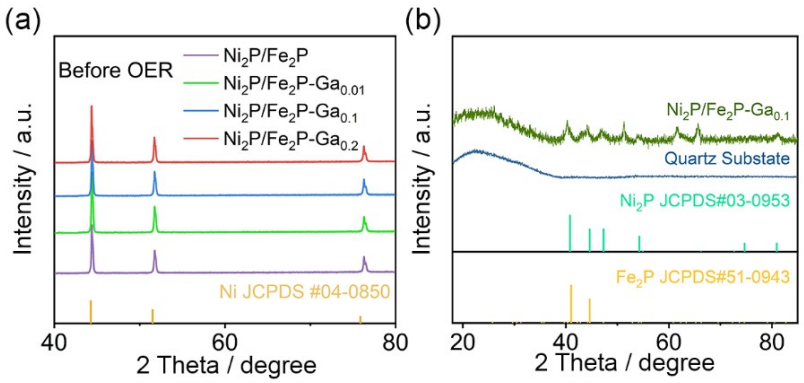

Fig. S4 XRD patterns of Ni_2P/Fe_2P-Ga grown on (a) a nickel mesh and (b) a quartz substrate.

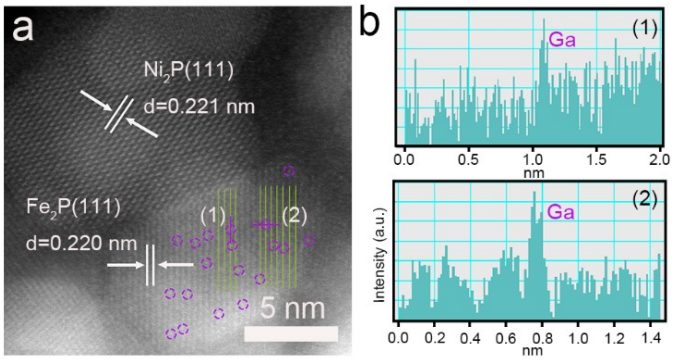

Fig. S5 (a) HAADF-STEM images and (b) the corresponding intensity line profiles of Ni_2P/Fe_2P-$Ga_{0.1}$.

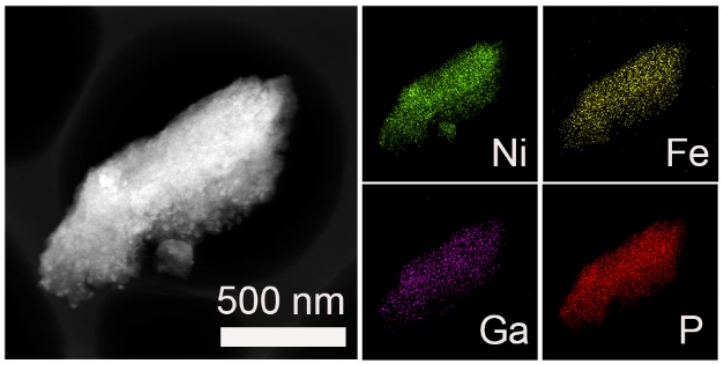

Fig. S6 The elemental mapping images of Ni_2P/Fe_2P-$Ga_{0.1}$.

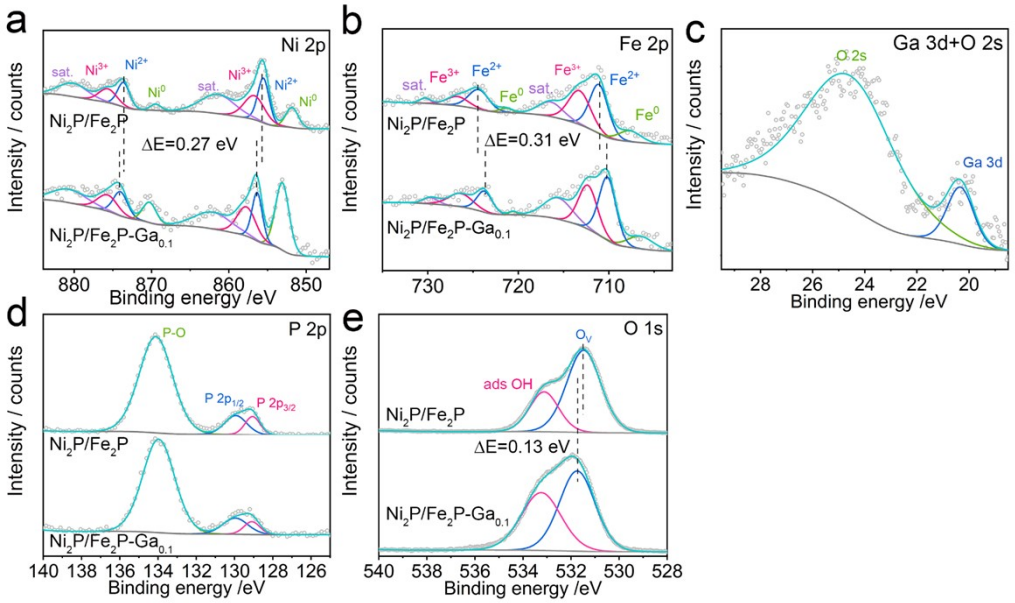

Fig. S7 High-resolution XPS spectra of Ni_2P/Fe_2P and Ni_2P/Fe_2P -$Ga_{0.1}$: (a) Ni 2p, (b) Fe 2p, (c) Ga 3d + O 2s, (d) P 2p, and (e) O 1s.

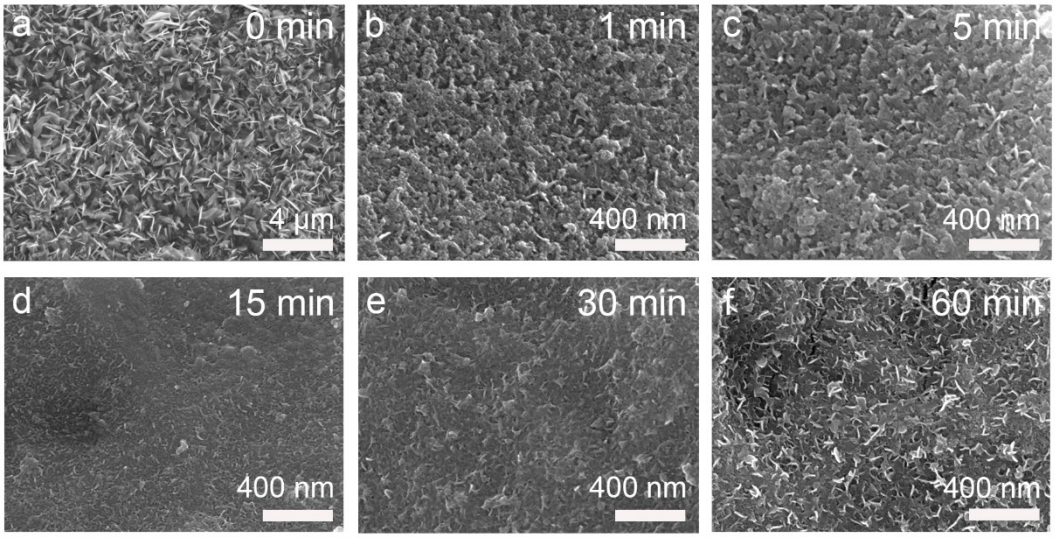

Fig. S8 SEM images of Ni_2P/Fe_2P-$Ga_{0.1}$ during OER process at 100 mA cm^{-2} for (a) 0 min, (b) 1 min, (c) 5 min, (d) 15 min, (e) 30 min, and (f) 60 min.

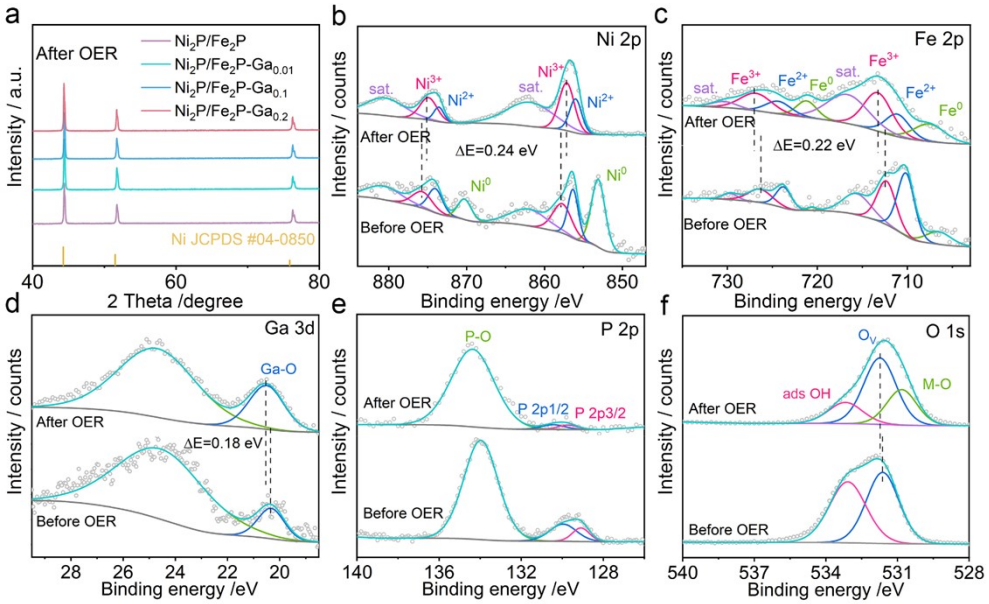

Fig. S9 (a) X-ray diffraction patterns of post-OER electrodes. XPS spectra of Ni_2P/Fe_2P-$Ga_{0.1}$ before and after OER: (b) Ni 2p, (c) Fe 2p, (d) Ga 3d + O 2s, (e) P 2p, and (f) O 1s.

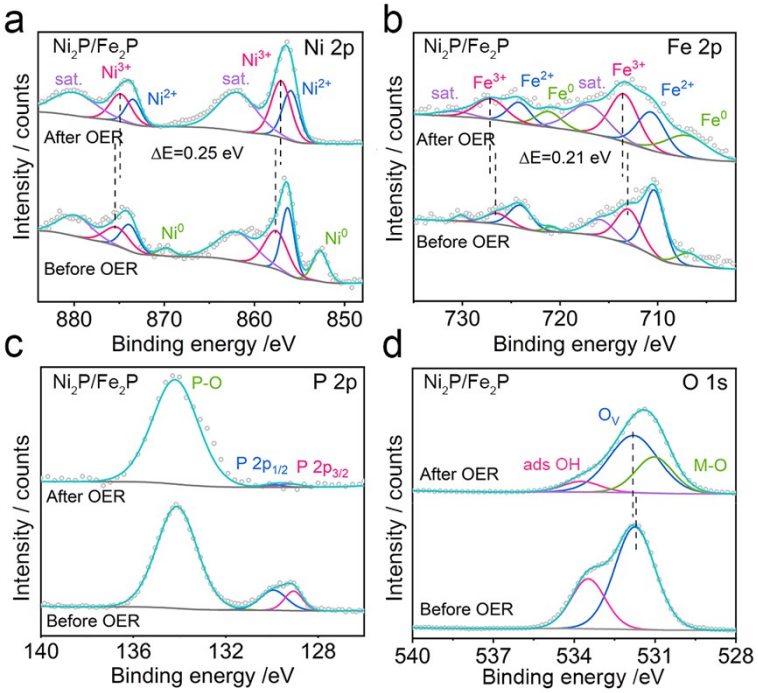

Fig. S10 XPS spectra of Ni_2P/Fe_2P before and after OER: (a) Ni 2p, (b) Fe 2p, (c) P 2p, and (d) O 1s.

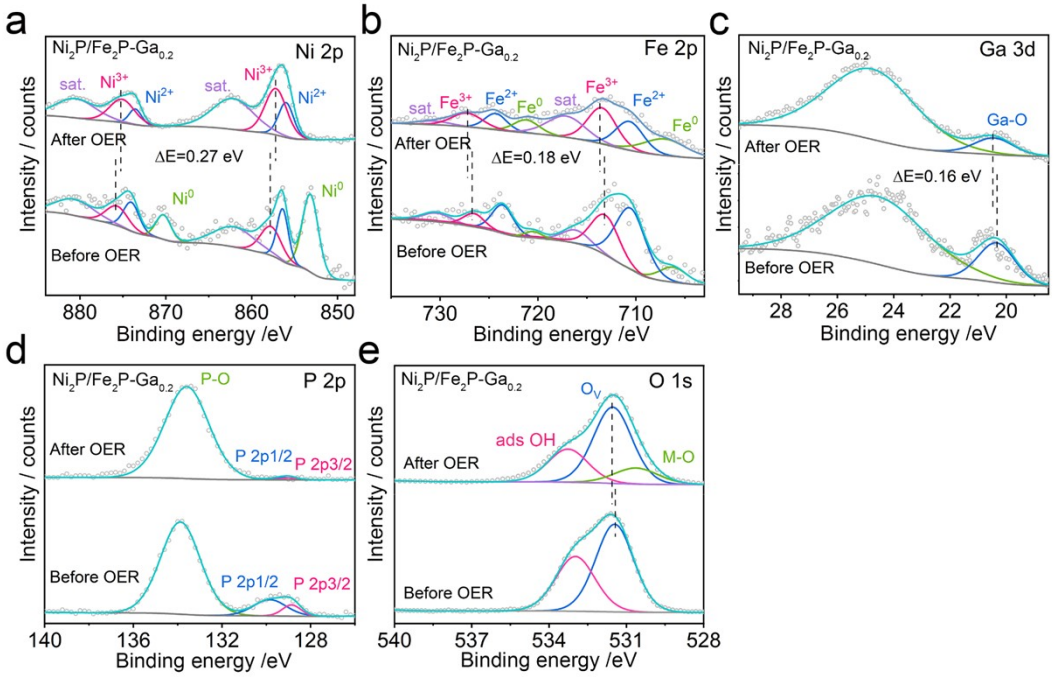

Fig. S11 XPS spectra of Ni_2P/Fe_2P-$Ga_{0.2}$ before and after OER: (a) Ni 2p, (b) Fe 2p, (c) Ga 3d + O 2s, (d) P 2p, and (e) O 1s.

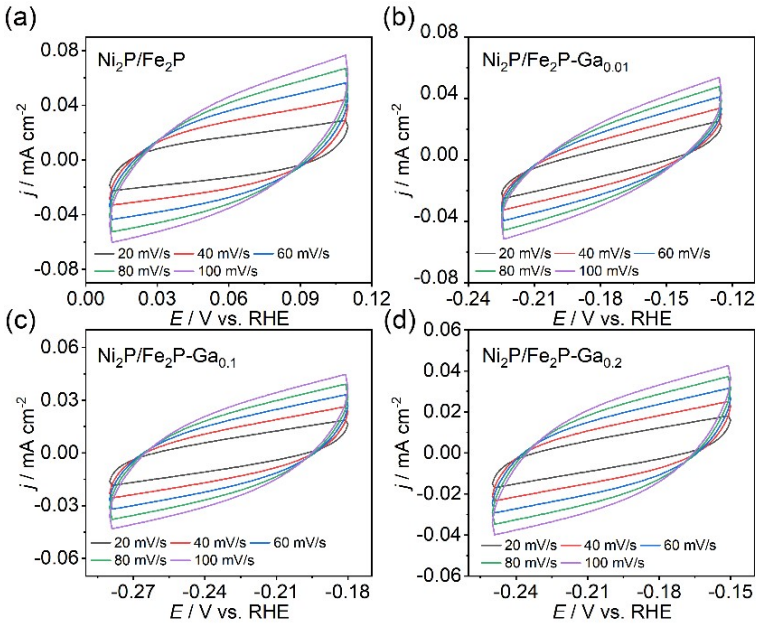

Fig. S12 CV curves for (a) Ni_2P/Fe_2P, (b) Ni_2P/Fe_2P-$Ga_{0.01}$, (c) Ni_2P/Fe_2P-$Ga_{0.1}$, and (d) Ni_2P/Fe_2P-$Ga_{0.2}$.

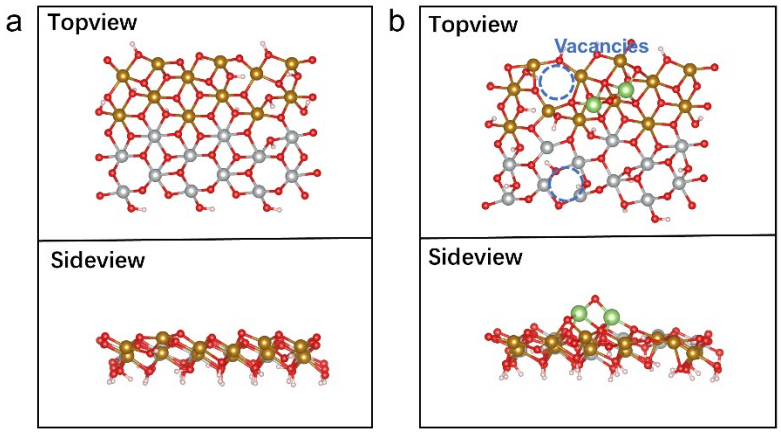

Fig. S13 The optimized structure of (a) NiFeOOH and (b) NiFeOOH-Ga_2O_3.

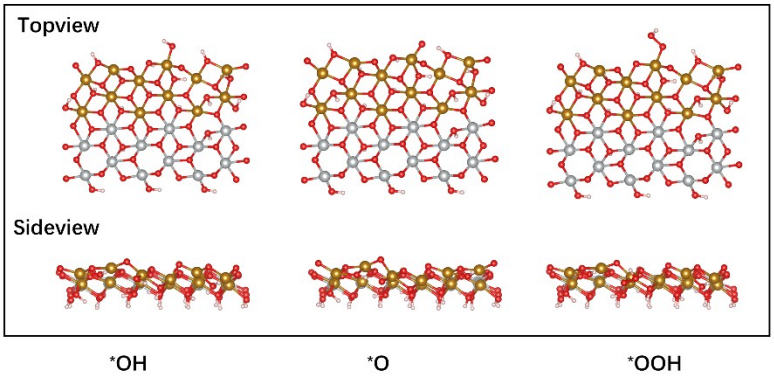

Fig. S14 The optimized OER configuration of reaction intermediates on NiFeOOH.

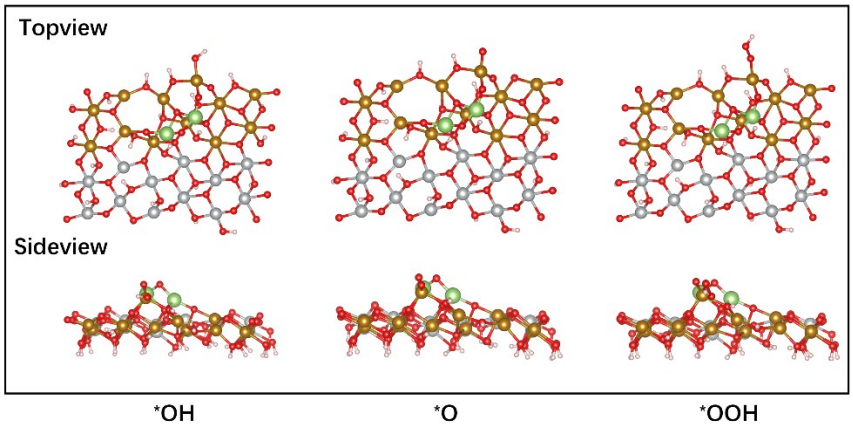

Fig. S15 The optimized OER configuration of reaction intermediates on NiFeOOH-Ga_2O_3.

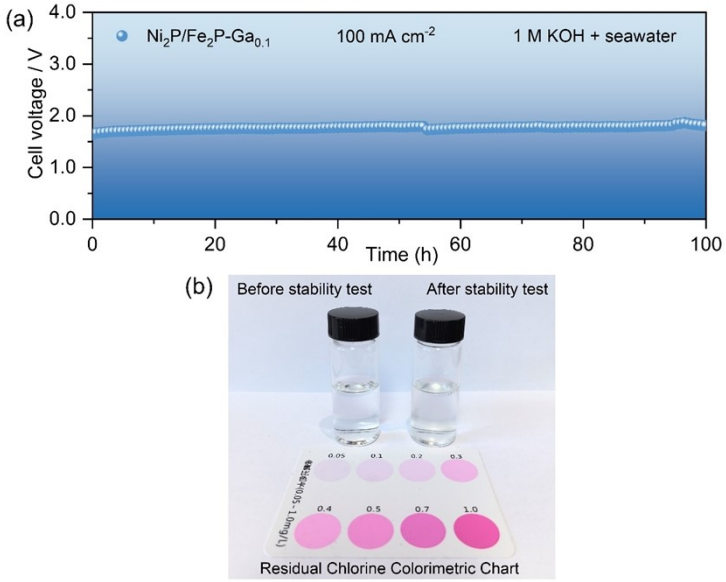

Fig. S16 (a) Chronopotentiometric test of an AEMWE cell assembled with Pt/C || Ni_2P/Fe_2P-$Ga_{0.1}$ at 100 mA cm^{-2} in 1 M KOH + seawater electrolyte. (b) Colorimetric test results for hypochlorite after 100 h stability test of the Ni_2P/Fe_2P-$Ga_{0.1}$ electrode at 100 mA cm^{-2}.

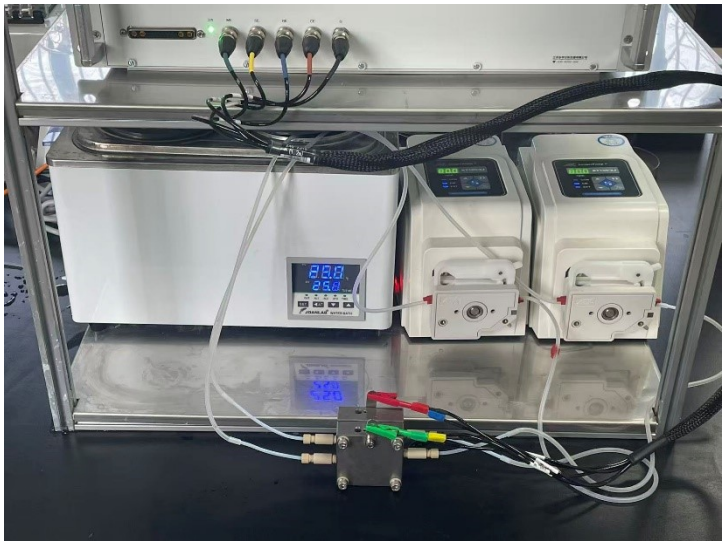

Fig. S17 The schematic diagram of the AEMWE system using Pt/C|| Ni_2P/Fe_2P-$Ga_{0.1}$.

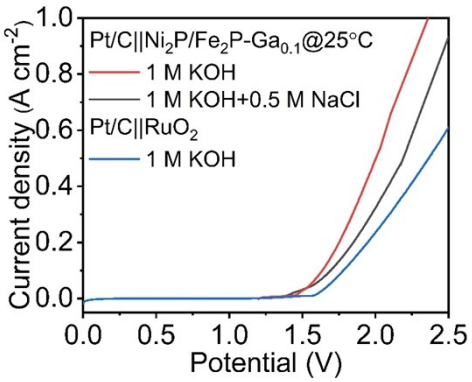

Fig. S18 The polarization curve of AEM electrolyzer using Pt/C || Ni_2P/Fe_2P-$Ga_{0.1}$ and Pt/C || RuO_2 at 25°C, respectively.

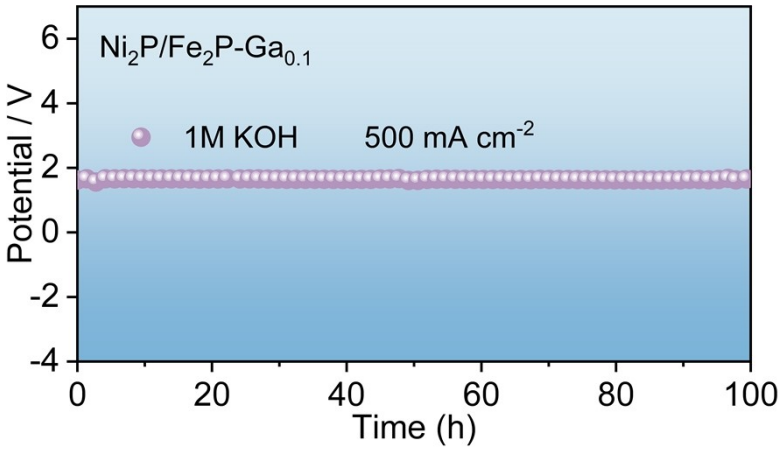

Fig. S19 Chronopotentiometric testing of the AEMWE using Pt/C || Ni_2P/Fe_2P-$Ga_{0.1}$ at 500 mA cm^{-2}.

Table S1 Overpotential comparison of recently reported OER electrocatalysts.

Catalyst	Loading (mg cm^{-2})	Overpotential (mV, j=100 mA cm^{-2})	Electrolyte	Refs.
Ni_2P/Fe_2P-$Ga_{0.1}$	0.63	227	1 M KOH	**This work**
		249	1M KOH+0.5 M NaCl	
$NiCe_{0.05}$/Fe@NM	6.2	257	1 M KOH	*Small* 2024, 2403971
CoNi-LDH/FeSe	~2.0	272	1 M KOH	*Chem. Eng. J.* 2024, 498, 155834.
		272	1 M KOH+0.5 M NaCl	
$Ni_3FeN@PO_4^{3-}$/NF	~1.8	258	1 M KOH	*Adv. Mater.* 2024, 2415421
CV-B-NiFe-LDH	N/A	219	1 M KOH	*J. Colloid Interface Sci.* 2024, 668, 607.
		236	1 M KOH+0.5 M NaCl	
NiFeCo(OH)	N/A	255.3	1 M KOH+1.0 M NaCl	*ACS Catal*. 2024, 14, 18322
FeMoOOH/NF	~5.0	240	1 M KOH	*Energy Environ. Sci*. 2025, 18, 1952
EA-$Ni_{0.82}Fe_{0.18}$-OH	N/A	250	1 M KOH+0.5 M NaCl	*J. Energy Chem*. 2024, 90, 486.
NiFe LDH-PANI	N/A	270	1 M KOH	*Appl. Catal. B: Environ. Energy*, 2021, 297, 120453.
$Fe_{2.5}Co_{2.5}Ni_{10}O_yH_z$@NFF	N/A	229	1 M KOH	*Carbon Energy* 2025, e684.
NiFe@NVG/CC	N/A	300	1 M KOH	*Nano Res.* 2024, 17, 4790
NiFeGa-LDH@NF	~1.25	258	1 M KOH	*J. Mater. Chem. A* 2025, 13, 16241
Ni_2P-$NiFe_2O_4$	0.25	305	1 M KOH	*Appl. Catal. B: Environ. Energy 2023,339, 123141*

Table S2 Comparison of AEMWE performance of Ni_2P/Fe_2P-$Ga_{0.1}$ with reported catalysts.

Catalyst	Loading (mg cm^{-2})	Conditions	Performance	Stability	Refs.
Pt/C|| Ni_2P/Fe_2P-$Ga_{0.1}$	0.5 || 0.63	85°C, 30 wt.% KOH	1.78V@500mA cm^{-2}	100 h@500mA cm^{-2} 1 M KOH + 0.5 M NaCl at 25°C	**This work**
FeRu@NM-2 || FeRu@NM-2	0.75 || 0.75	60°C, 1 M KOH	1.89V@400mA cm^{-2}	300 h @500mA cm^{-2} 1 M KOH at 60°C	*Chem. Eng. J.* 2024, 493, 152547.
$NiCe_{0.05}$/Fe@NM ||$NiCe_{0.05}$/Fe@NM	6.2 || 6.2	60°C, 5 M KOH	1.825V@300mA cm^{-2}	100 h@500mA cm^{-2} 5 M KOH at 60°C	*Small* 2024, 2403971
$Ni_3FeN@PO_4^{3-}$ /NF||Pt-Ni@MoN/NF	1.8 || N/A	25°C, 1 M KOH + seawater	1.95V@500mA cm^{-2}	200 h@500mA cm^{-2} 1 M KOH + seawater at 25°C	*Adv. Mater.* 2024, 2415421
$Co_{2.8}W_{3.8}$-NiFe LDH||Pt/C	N/A	60°C, 1 M KOH	1.86V@1000mA cm^{-2}	300 h@1000mA cm^{-2} (1 M KOH at 60°C)	*Adv. Energy Mater.* 2024, 14, 2402046.
CuNi@NiSe || CuNi@NiSe	N/A	80°C, 1 M KOH	2.0V@500 mA cm^{-2}	10 h@100mA cm^{-2} (1 M KOH at 80°C)	*Small* 2023, 19, 2301613.